

Supporting Information

Wavelength-Resolved Near Infra-red Light Induced Free-Radical Polymerization

Philipp Neidinger,^{a,b} Joshua Davis,^b Joshua A. Carroll,^b Jochen Kammerer,^b Esa Jaatinen,^b Sarah L. Walden,^{b,c,d*}
Andreas-Neil Unterreiner^{a*} and Christopher Barner-Kowollik^{*a,b,e}

^a Institute of Physical Chemistry, Karlsruhe Institute of Technology (KIT), Fritz-Haber-Weg 2, 76131 Karlsruhe, Germany.

^b School of Chemistry and Physics, Queensland University of Technology (QUT), 2 George Street, Brisbane, QLD 4000 Australia Address here.

^c Institute of Solid State Physics, Abbe Center of Photonics, Helmholtzweg 3, Friedrich Schiller University Jena, 07743 Jena, Germany

^d Institute of Applied Physics, Abbe Center of Photonics, Albert-Einstein-Str. 15, Friedrich Schiller University Jena, 07745 Jena, Germany

^e Institute of Nanotechnology, Karlsruhe Institute of Technology (KIT), Hermann-von-Helmholtz-Platz 1, 76297 Eggenstein-Leopoldshafen, Germany

Abstract

Initiating polymerization processes at long wavelengths, ideally in the near-infrared (NIR) range, is critical to enable applications where shorter wavelengths may be harmful and where high penetration depths may be required. While we have recently demonstrated that gold nanorods (AuNR) function as effective photothermal converters at 800 nm to initiate free radical polymerizations, a careful wavelength-by-wavelength assessment (action plot analysis) of their effectiveness is outstanding. Herein, we provide a full NIR action plot from 620 to 950 nm, probing the wavelength-by-wavelength monomer to polymer conversion at an identical number of photons at each wavelength. While the vast majority of action plots show a red-shift relative to the absorption spectrum, we herein observe a pronounced blue-shift for the most effective conversion.

Table of Contents

1 Theoretical Considerations.....	3
2 Experimental Procedures	4
2.1 Laser System.....	4
2.2 Materials.....	4
2.3 Characterization	4
2.3.1 Nuclear Magnetic Resonance Spectroscopy	4
2.3.2 Gel Permeation Chromatography/Size Exclusion Chromatography	4
2.3.3 UV/Vis/NIR Spectroscopy	4
2.4 Action Plots.....	4
3 Additional Experimental Data	5
3.1 Absorption spectrum of AuNR	5
3.2 Action Plot Energy Calculation	7
3.3 NMR Spectroscopy	7
3.3.1 Determination of Monomer to Polymer Conversion	7
3.3.2 NMR Spectra Analysis.....	8
3.4 Size Exclusion Chromatography	10
3.5 Transmission Electron Microscopy (TEM)	11
4 References.....	13

1 Theoretical Considerations

The simulations for the NRs temperature evolution were completed using the finite element method in COMSOL Multiphysics, solving the system of diffusion equations presented by Metwally and colleagues.¹ There are three stages of heating for a nanoparticle and its surrounding medium for a pulsed laser, these stages are, (1) electronic absorption, (2) electron-phonon thermalization and (3) external heat diffusion.² Electronic absorption occurs on a time scale of $\tau_e \approx 100$ fs, while electron-phonon thermalization occurs at $\tau_{e-ph} \approx 1.7$ ps for gold and for external heat diffusion the timescale is hundreds of ps to a few ns depending on the particle size. In our previous work,³ where the pulse duration was on the fs scale, these processes occur sequentially, however in the case of the 5 ns pulses used here this is no longer the case. As such a source term of

$$S(t) = \frac{\sigma_{abs} F}{V \tau_p} e^{-\pi \frac{(t-t_0)^2}{\tau_p^2}},$$

was used instead of the initial temperature change that was used in our previous report.³ σ_{abs} is the absorption cross section, F is the fluence, V the volume of the NR, τ_p the full width half maximum duration of the pulse and t_0 the time at which the pulses peak intensity occurs. The source term requires knowledge of the absorption cross section, which is also calculated with COMSOL Multiphysics. Absorption and scatter cross sections in NRs have both a longitudinal and transverse resonance which have different cross sections and resonance peaks. Given the excitation wavelength is always longer than where the transverse resonance occurs, only the longitudinal resonance is simulated.

While the simulations are based on the method given in,¹ due to the asymmetry of NRs compared to spherical nanoparticles the diffusion equation was solved in three dimensions. It is assumed here that the temperature of the NR is uniform; while this is not strictly correct, it provides a reasonable approximation, particularly in this application where the temperature of the medium determines polymerization, rather than the temperature of the NR. Finally, it is important to note that there is a temperature discontinuity at the surface of the NR due to the interfacial resistance, known as the Kapitza resistance.⁴

2 Experimental Procedures

2.1 Laser System

A tuneable ns laser system Coherent Opolette 355 with a pulse duration of 7 ns and a repetition rate of 20 Hz served as light source. A combination of computer-controlled Second Harmonic Generation (SHG), Third Harmonic Generation (THG) and Optical Parametric Oscillator (OPO) systems enabled the continuous tunability of the output wavelength.

2.2 Materials

N,N-dimethylacrylamide (DMA, 99%, contains 500 ppm monomethyl ether hydroquinone (MEHQ) as inhibitor, Sigma-Aldrich), azoisobutyronitrile (AIBN, 98%, Sigma-Aldrich), 3-mercaptopropionic acid (99%, Sigma-Aldrich), gold nanorods AuNR (800 nm, OD=1, bare citrate, Biozol)

2.3 Characterization

2.3.1 Nuclear Magnetic Resonance (NMR) Spectroscopy

The structures of the synthesized polymers were confirmed *via* ^1H -NMR spectroscopy using a Bruker Ascend 600 MHz spectrometer for hydrogen nuclei. Samples were dissolved in D_2O . The δ -scale was referenced with tetramethylsilane ($\delta = 0.00$) as internal standard.

2.3.2 Gel Permeation Chromatography/Size Exclusion Chromatography (SEC)

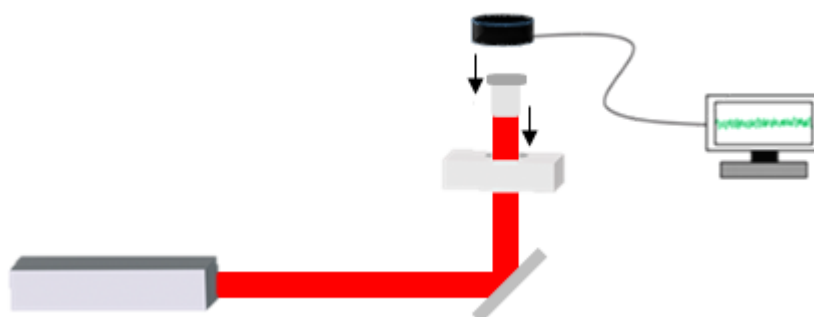
SEC measurements were performed on a PSS SECurity² system that consists of a PSS SECurity Degasser, a PSS SECurity TCC6000 Column Oven and a PSS GRAM Column Set with 8 x 150 mm 10 μm Precolumn and 8 x 300 mm 10 μm Analytical Columns. The device further consists of an Agilent 1260 Infinity Isocratic Pump, and Agilent 1260 Infinity Standard Autosampler, an Agilent 1260 Infinity Diode Array, and a refractive index detector. HPLC grade DMAc with 0.01 M LiBr was used as solvent at a flow rate of 1 mL min^{-1} . Poly(methyl methacrylate) standards were used as calibrants.

2.3.3 UV/Vis/NIR Spectroscopy

UV/Vis/NIR spectra were recorded in quartz cuvettes (optical path length 1 cm) on a Varian Cary 500 spectrophotometer at a spectral resolution of 1 nm.

2.4 Action Plots

The general action plot methodology has been described before (see supporting information of ref.⁵) and is briefly reiterated herein. 150 μL aliquots were taken from a bulk solution of AIBN dissolved in DMA into a glass vial with 7 mm diameter and filled up with 75 μL isopropanol, 75 μL AuNR solution and 10 μL 3-mercaptopropionic acid, such that each sample of 300 μL solution had a concentration of 4.85 mol L^{-1} DMA, 3.53 mol L^{-1} isopropanol and 0.01 mol L^{-1} AIBN. The glass vials were capped and placed in an in-house built metal sample holder with a central hole to be irradiated from below (refer to Scheme S1). The output beam of the tuneable ns laser was aligned via a lens system to control the beam diameter and subsequently redirected 90° upwards by a prism.



Scheme S1: Setup of the tuneable ns laser action plot experiments. The laser beam is 90° redirected from a parallel flat to the optical bench. Thus, a vial which is placed into an in-house built sample holder can be irradiated from below. The NIR wavelength can be automatically tuned by a computer-controlled OPO. The incident laser beam energy was measured by a photodiode connected with a power meter.

3 Additional Experimental Data

3.1 Absorption spectrum of AuNR

For the action plot experiments, we purchased AuNR with equivalent properties (nanocomposix, NanoXact Gold Nanorods - Bare (Citrate), $\lambda_{max} = 800 \text{ nm}$, $OD = 1$) as the ones that we used for the proof-of-principle experiment with the fs laser in our previous publication³ and the femtosecond reshaping experiments included in the current work. However, the AuNR dimensions can vary from batch-to-batch. To ensure that the physical properties are comparable, we measured absorption spectra of both batches. As depicted in Figure S1, both the absorption spectrum of the AuNR used for the femtosecond experiments (red) and the nanosecond experiments (black) show almost identical trends with the transversal peak at approximately 500 nm and the longitudinal peak at close to 800 nm. Thus, we conclude that the AuNR of both solutions are comparable under irradiation with identical conditions.

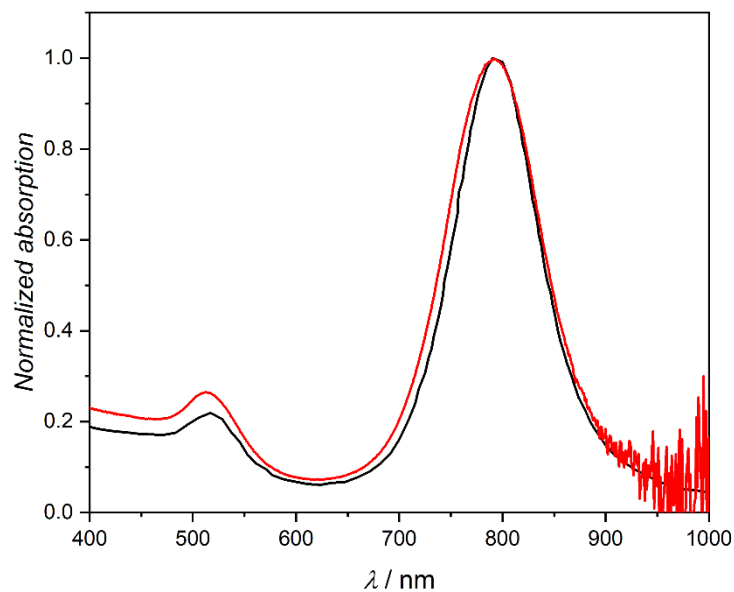


Figure S1: Normalized absorption spectrum of the AuNR that were used in our previous report under fs laser irradiation (red),² and normalized absorption spectrum of the AuNR that were used for the action plot measurements in the current ns laser based report (black). Both spectra are almost identical with peak absorption of the transversal band between 500 nm and 600 nm and the longitudinal band between 700 and 900 nm.

As a control experiment to assess whether the observed blue-shift in the action originates from reshaping of the AuNR, we recorded time-dependent absorption spectra of the reaction solution under identical conditions as for the action plot experiments (800 nm, 260 μJ). As depicted in Figure S2, we observe a weak redshift in the absorption spectrum during 15 min irradiation time. We also repeated the same experiment under femtosecond irradiation (35 fs, 1 kHz, 25 GW cm^{-2}) to confirm the setup can reproduce literature known effects of femtosecond-induced AuNR reshaping.⁶ The expected blue-shift due to AuNR reshaping can be seen in Figure S3.

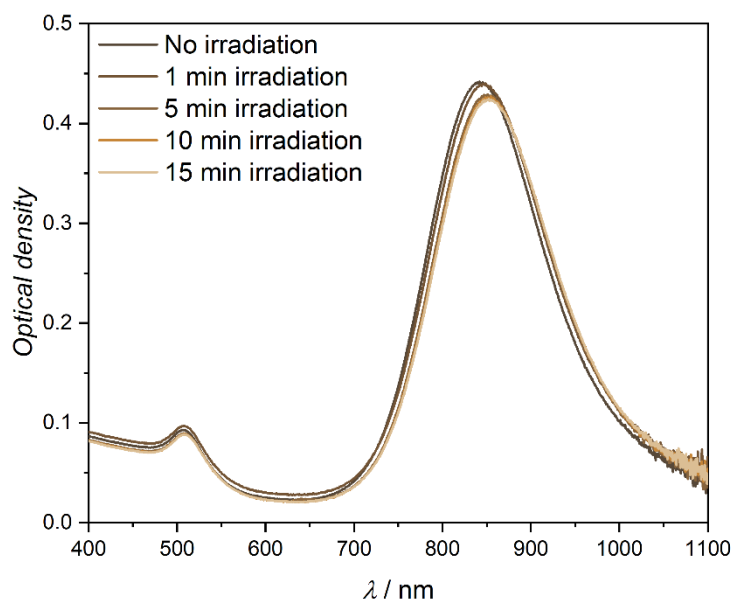


Figure S2: Absorption spectra of a solution of 4.85 mol L⁻¹ DMA, 3.53 mol L⁻¹ isopropanol, 75 μL AuNR in water. From dark to pale: Absorption spectrum of the solution immediately after preparation without irradiation, after 1 min irradiation, after 5 min irradiation, after 10 min irradiation and after 15 min irradiation with 10 ns pulses at 800 nm with 260 μJ.

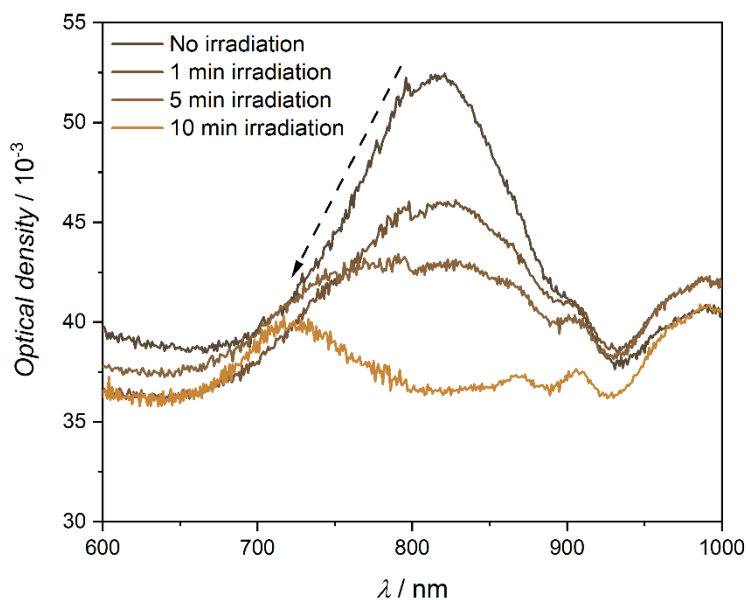


Figure S3: Absorption spectra of a solution of 4.85 mol L⁻¹ DMA, 3.53 mol L⁻¹ isopropanol, 0.01 mol L⁻¹ AIBN, 75 μL AuNR in water and 10 μL (0.38 mol L⁻¹) 3-mercaptopropionic acid. From dark to pale: Absorption spectrum without irradiation, absorption spectrum after 1 min irradiation, absorption spectrum after 5 min irradiation, absorption spectrum after 10 min irradiation with 170 fs pulses at 800 nm with 250 μJ. The black dashed arrow indicates the blue shift of the absorption maximum during the increasing longer irradiation times.

3.2 Action Plot Energy Calculation

The number of photons was controlled via a calculated pulse energy at each specific wavelength and via a shutter placed between the telescope and the prism to precisely control the irradiation time. The number of photons n_p for a monochromatic light source is given by the Planck-Einstein equation

$$n_p = \frac{E_{pulse} \lambda}{h \cdot c \cdot N_A} \quad (1)$$

Here, E_{pulse} is the energy of the laser pulses, λ the wavelength, h is Planck's constant, c is the speed of light and N_A is Avogadro's constant. By means of the equation the target energy for each wavelength can be calculated for a defined number of photons. This procedure guarantees the above-mentioned identical number of photons penetrating the sample for each experiment at different wavelengths. However, the energy was measured before inserted into the sample vial. Since the glass vial absorb and scatters light, the beam energy may decrease while penetrating the samples. The 'effective' energy in the sample is then given by

$$E_0 = \frac{n_p \cdot N_A \cdot h \cdot c}{k \cdot T_\lambda \cdot \lambda} \quad (2)$$

where T_λ is the wavelength dependent transmittance. In the wavelength region used in the current work, the transmission of the glass vials is constant⁷ and the wavelength dependent solvent absorption is negligible.^{8,9} Therefore, T_λ can be neglected in Eqn. (2).

Table S1. Overview of wavelength-dependent energy for the action plot.

Wavelength / nm	Energy / μJ
950	219
840	248
820	254
800	260
780	267
760	274
740	281
720	289
700	297
680	306
660	315
640	325
620	335

3.3 NMR Spectroscopy

3.3.1 Determination of Monomer to Polymer Conversion

Figure S4 displays the ^1H NMR spectrum of a sample of 4.04 mol L^{-1} DMA with 9 mmol L^{-1} AIBN, $100 \mu\text{L}$ AuNR solution and $10^{-2} \text{ mol L}^{-1}$ CTA dissolved in $250 \mu\text{L}$ D_2O prior to irradiation (A) and after 30 min irradiation with 25 GW cm^{-2} at 800 nm (B).

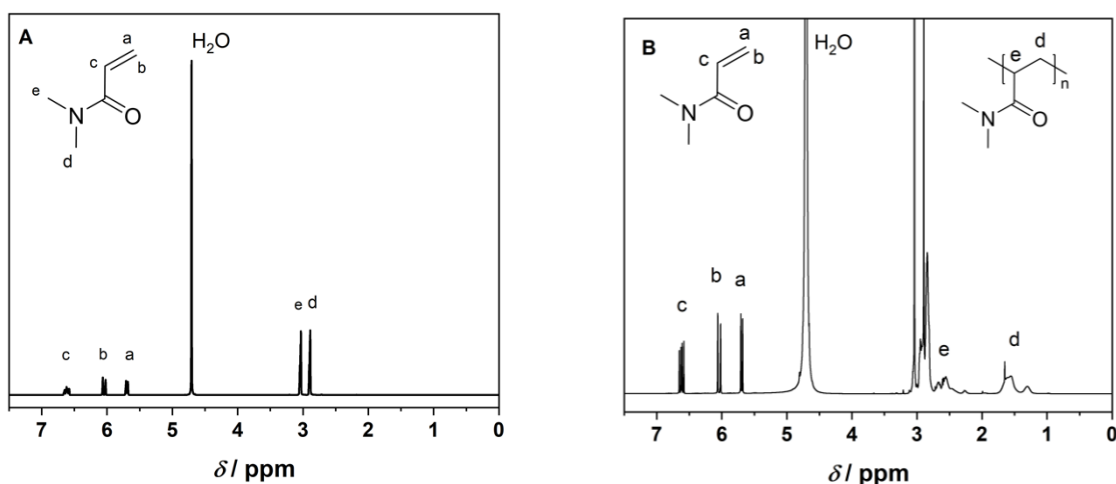


Figure S4: (A) ¹H NMR spectrum of pure DMA dissolved in D₂O without irradiation. The resonances are assigned to the protons of DMA; (B) ¹H NMR spectrum of a solution of DMA, AIBN, AuNR and CTA dissolved in D₂O after irradiation of 30 min. The resonances are assigned to the protons associated with the DMA monomer and the generated polymer.

Since the sample was not irradiated and thus there was no polymer formation, all resonances are assigned to protons of the monomer in (a). In (b) additional resonances are visible that are associated with the generated polymer. The monomer to polymer conversion can be determined by the ratio of the integrals that are assigned to the polymer resonances and the sum of the integrals of both the polymer and the monomer resonances.

$$\text{Conversion} = \frac{f(d)}{f(a)+f(b)+f(d)} * 100\%$$

The polymer resonances close to 2.5 – 3 ppm ((B), e) are not suitable for the calculation of conversion as they are overlapping with the monomer associated resonances at 3 ppm. The polymer associated resonances between 1 and 2 ppm (d), however, are well separated from the monomer signals, allowing their use as reference signals for the calculation of the monomer to polymer conversion. Considering that the monomer resonances a and b are the analogue protons to the protons d in the polymer, the monomer conversion can be readily calculated by rationing the polymer resonances d and the sum of d and the monomer resonances a and b.

3.3.2 NMR Spectra Analysis

For each wavelength the conversion was measured triplicate via ¹H-NMR spectroscopy to determine the average conversion with an error resulting from the standard deviation the average conversion.

Table S2. Overview of the conversion of the single action plot experiments as well as the average conversion and data error, given by the standard deviation of the average conversion, at each wavelength.

Wavelength / nm	Conversion 1 / %	Conversion 2 / %	Conversion 3 / %	Average Conversion / %	Error / %
620	0	0	0	0	0
640	8.5	7.7		8.1	0.6
660	12.9	11.4		12.2	1.1
680	14.4	11.4	8.5	11.4	2.9
700	11.4	17.2		14.3	4.1
720	24.9	22.9	19.4	22.4	1.4
740	34.9	30.0	37.4	34.2	3.0
760	36.3	38.9	35.4	36.8	1.5
780	32.0	34.5	27.9	31.4	3.3
800	33.3	23.5	25.6	30.4	4.2
820	25.2	19.5	23.5	22.7	2.9
840	11.8	11.8	11.4	11.7	0.2
950	0	0	0	0	0

Figure S5 shows stacked $^1\text{H-NMR}$ spectra of the reaction solutions after irradiation with each wavelength (identical number of photons) used in the action plot. Since the polymer formation is indicated by the resonances between 0-3.5 ppm (refer to Supporting Information section 3.3.1), Figure S6 depicts a zoom into this region of the spectrum, clearly demonstrating the evolution of the polymer associated resonances.

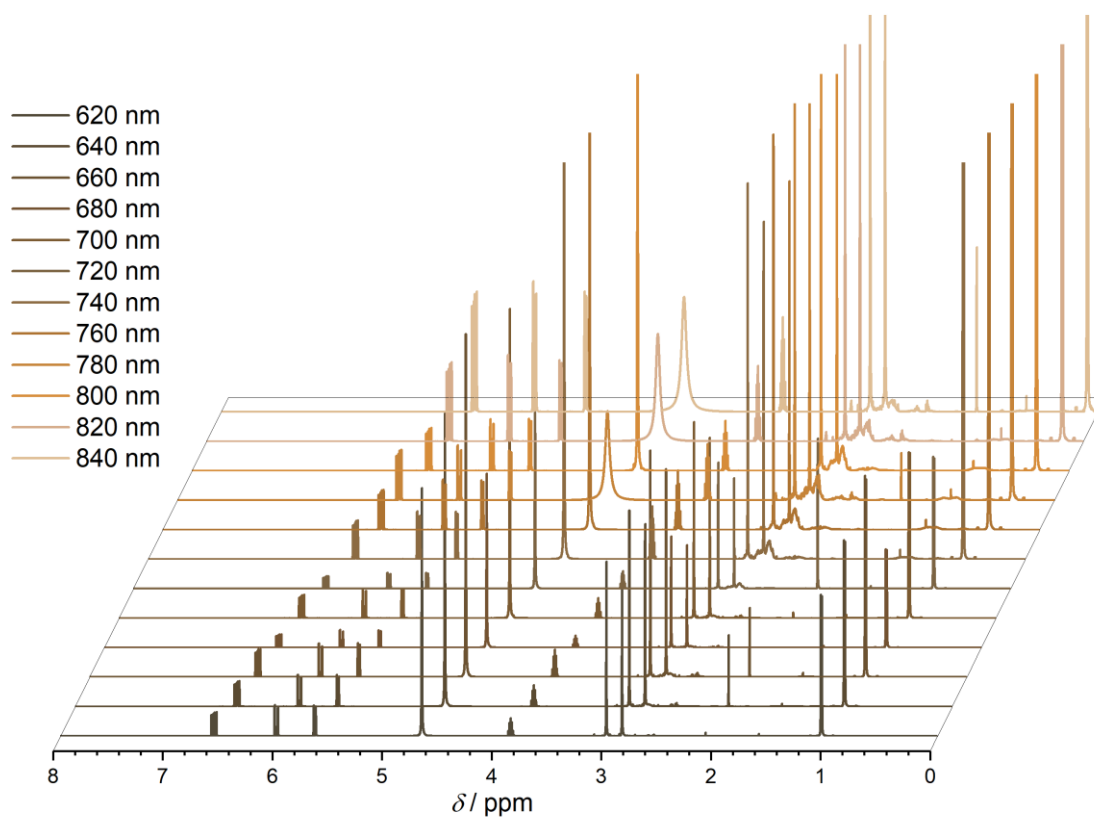


Figure S5: Stacked $^1\text{H-NMR}$ spectra of a solution with 4.85 mol L^{-1} DMA, 0.01 mol L^{-1} AIBN, 3.53 mol L^{-1} isopropanol, $75 \mu\text{L}$ AuNR and $10 \mu\text{L}$ (0.38 mol L^{-1}) CTA, irradiated with 10 ns pulses for 15 min, with (from dark to pale): $335 \mu\text{J}$ at 620 nm, $325 \mu\text{J}$ at 640 nm, $315 \mu\text{J}$ at 660 nm, $306 \mu\text{J}$ at 680 nm, $297 \mu\text{J}$ at 700 nm, $289 \mu\text{J}$ at 720 nm, $281 \mu\text{J}$ at 740 nm, $274 \mu\text{J}$ at 760 nm, $267 \mu\text{J}$ at 780 nm, $260 \mu\text{J}$ at 800 nm, $254 \mu\text{J}$ at 820 nm and $248 \mu\text{J}$ at 840 nm.

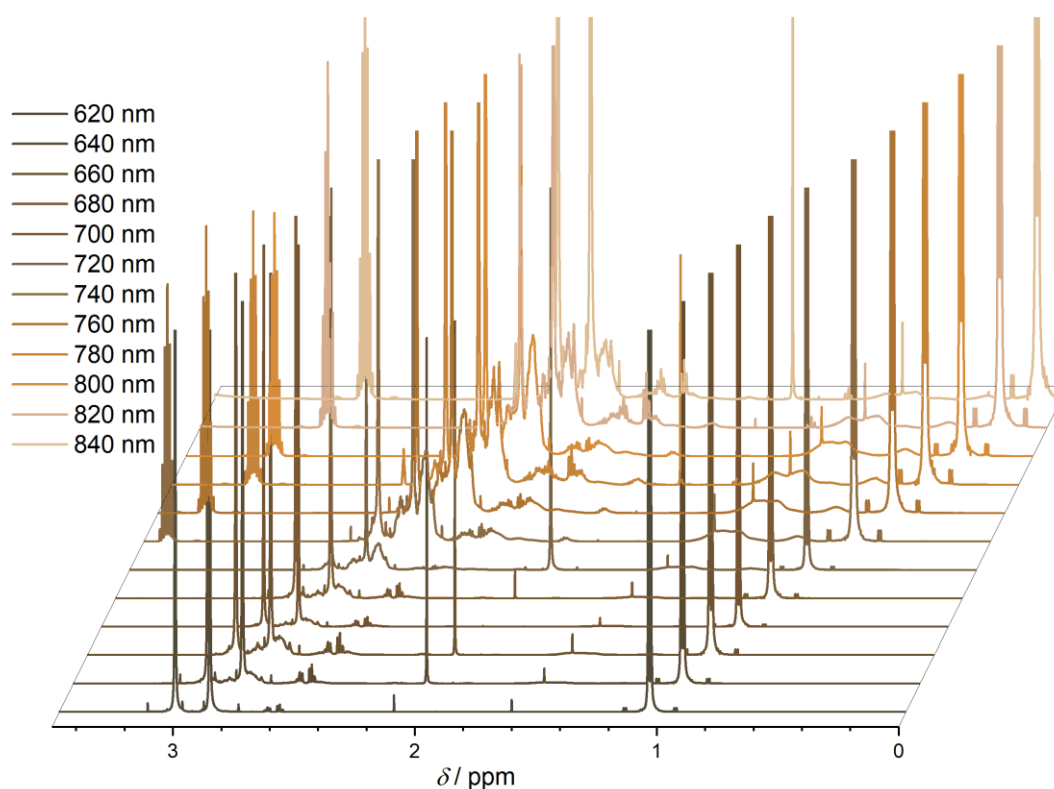


Figure S6: Stacked ^1H -NMR spectra of solution with 4.85 mol L^{-1} DMA, 0.01 mol L^{-1} AIBN, 3.53 mol L^{-1} isopropanol, $75 \mu\text{L}$ AuNR and $10 \mu\text{L}$ (0.38 mol L^{-1}) CTA, irradiated with 10 ns pulses for 15 min, with (from dark to pale): $335 \mu\text{J}$ at 620 nm, $325 \mu\text{J}$ at 640 nm, $315 \mu\text{J}$ at 660 nm, $306 \mu\text{J}$ at 680 nm, $297 \mu\text{J}$ at 700 nm, $289 \mu\text{J}$ at 720 nm, $281 \mu\text{J}$ at 740 nm, $274 \mu\text{J}$ at 760 nm, $267 \mu\text{J}$ at 780 nm, $260 \mu\text{J}$ at 800 nm, $254 \mu\text{J}$ at 820 nm and $248 \mu\text{J}$ at 840 nm. Zoom into region 0-3.5 ppm.

3.4 Size Exclusion Chromatography

The wavelength-dependent peak molecular weight M_p , as depicted in Figure 2 of the manuscript, was determined using SEC with an error of 20 % for each data point, which is an accepted error range for SEC molecular weight determination without an absolute molecular weight method. An overview of the M_p and error data is provided in Table S3. Figure S7 shows the recorded SEC traces.

Table S3: Overview of the peak molecular of the single action plot experiments and data error, given by the systematic error of the instrument.

Wavelength / nm	$M_p / \text{g mol}^{-1}$	Error / g mol^{-1}
620	250	50
640	350	70
660	250	50
680	230	50
700	250	50
720	1250	250
740	1700	340
760	1600	310
780	1750	350
800	1600	320
820	1800	360
840	1400	280

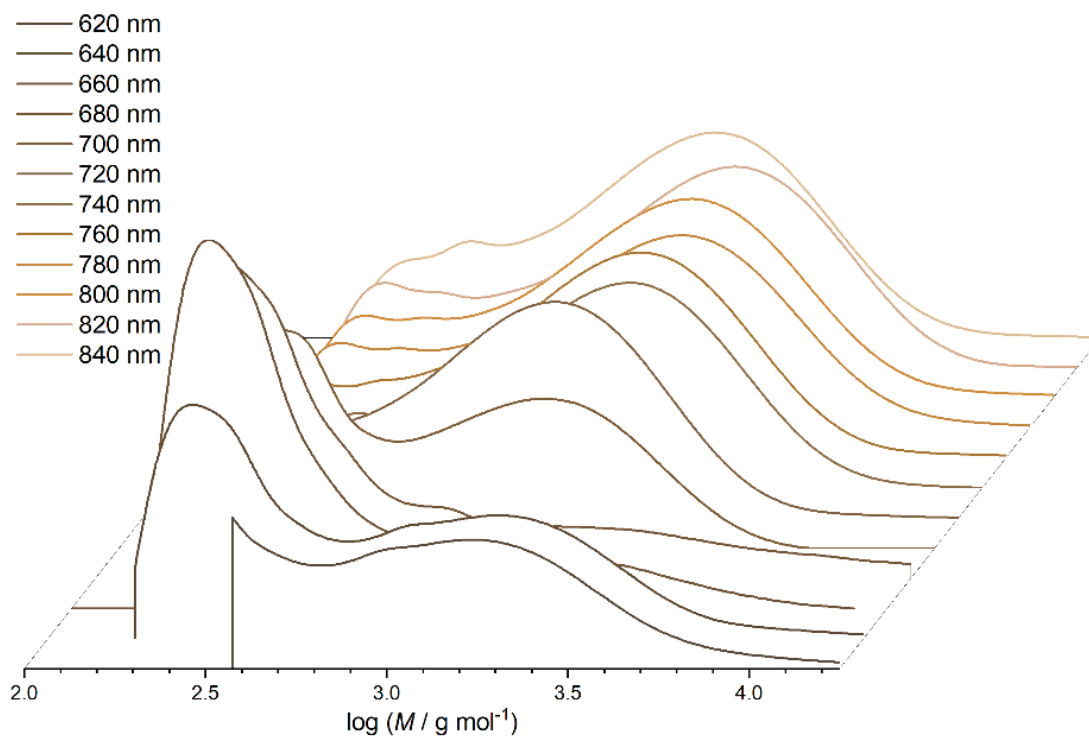


Figure S7: Stacked SEC traces of PDMA and DMA after 15 min irradiation of a solution with 4.85 mol L⁻¹ DMA, 3.53 mol L⁻¹ isopropanol, 0.01 mol L⁻¹ AIBN, 75 μ L AuNR solution and 10 μ L 3-mercaptopropionic acid with a 10 ns laser with (from dark to pale) 335 μ J at 620 nm, 325 μ J at 640 nm, 315 μ J at 660 nm, 306 μ J at 680 nm, 297 μ J at 700 nm, 289 μ J at 720 nm, 281 μ J at 740 nm, 274 μ J at 760 nm, 267 μ J at 780 nm, 260 μ J at 800 nm, 254 μ J at 820 nm and 248 μ J at 840 nm.

3.5 Transmission Electron Microscopy (TEM)

4 μ L of the reaction mixture with and without 3-mercaptopropionic acid (MPA) were deposited on glow discharged carbon film TEM gold grids. Gold was chosen over standard copper grids to avoid the reaction of MPA with copper. The mixtures were plotted off with a filter paper after about 2 minutes and left to dry. The bright field images were acquired on a JEOL1400 transmission electron microscope operating at 120 kV with a TVIPS F4216 2K CCD camera.

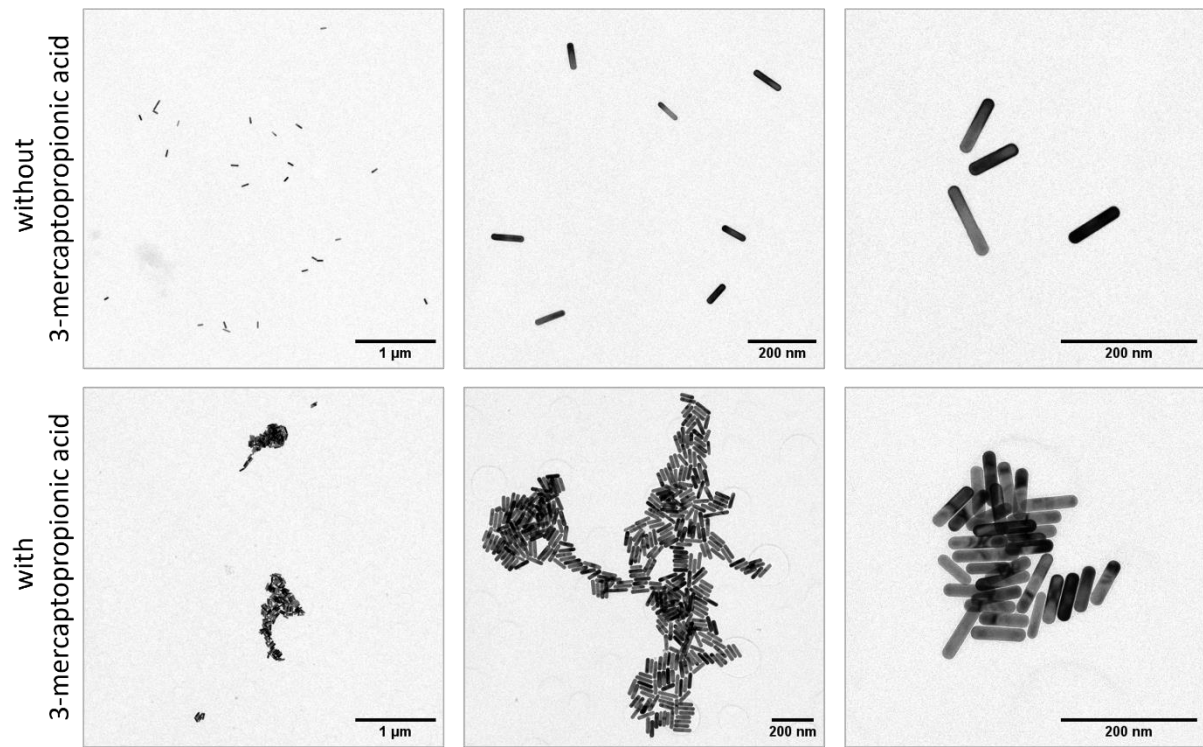


Figure S8: 3-mercaptopropionic acid (MPA) causes agglomeration of the AuNPs. The brightfield TEM images in the top row show the dispersion to individual AuNPs in the reaction solution without MPA. The AuNPs form agglomerates of random shape and number of NPs upon the addition of MDA (bottom row).

4 References

- 1 K. Metwally, S. Mensah and G. Baffou, *J. Phys. Chem. C*, 2015, **119**, 28586-28596.
- 2 A. Siems, S. A. L. Weber, J. Boneberg and A. Plech, *New J. Phys.*, 2011, **13**, 043018.
- 3 P. Neidinger, J. Davis, D. Voll, E. A. Jaatinen, S. L. Walden, A.-N. Unterreiner and C. Barner-Kowollik, *Angew. Chem., Int. Ed.*, 2022, **61**, e202209177.
- 4 G. Baffou and R. Quidant, *Laser Photonics Rev.*, **2013**, *7*, 171-187.
- 5 J. P. Menzel, B. B. Noble, A. Lauer, M. L. Coote, J. P. Blinco and C. Barner-Kowollik, *J. Am. Chem. Soc.*, 2017 **139**, 15812-15820.
- 6 S. Link and M. A. El-Sayed, *J. Phys. Chem. B*, 1999, **103**, 4212-4217.
- 7 S. L. Walden, H. Frisch, B. V. Unterreiner, A.-N. Unterreiner and C. Barner-Kowollik, *J. Chem. Ed.*, 2019, **97**, 543-548.
- 8 J. A. Curcio and C. C. Petty, *JOSA*, 1951, **41**, 302-304.
- 9 E. Sani and A. Dell'Oro, *Optical Materials*, 2016, **60**, 137-141.